encit 2020

ABCM Associação Brasileira de Engenharia e Ciências Mecânicas

18th Brazilian Congress of Thermal Sciences and Engineering
November 16-20, 2020 (Online)

ENCIT2020-0047
THERMODYNAMIC ANALYSIS OF THERMOMAGNETIC MOTORS

Luiz Felipe Avelar Lima
Deparment of Mechanical Engineering. Federal University of Minas Gerais, Av. Antônio Carlos, 6627 – Pampulha. ZIP 31270-901. Belo Horizonte, MG, Brazil.
luiz.avelar25@gmail.com

Matheus Urquiza Lima Santos
Deparment of Mechanical Engineering. Federal University of Minas Gerais, Av. Antônio Carlos, 6627 – Pampulha. ZIP 31270-901. Belo Horizonte, MG, Brazil.
urq.matheus@gmail.com

Lorenzo dos Santos Correa
Deparment of Mechanical Engineering. Federal University of Minas Gerais, Av. Antônio Carlos, 6627 – Pampulha. ZIP 31270-901. Belo Horizonte, MG, Brazil.
lorenzocorrea6@gmail.com

Paulo V. Trevizoli
Deparment of Mechanical Engineering. Federal University of Minas Gerais, Av. Antônio Carlos, 6627 – Pampulha. ZIP 31270-901. Belo Horizonte, MG, Brazil
trevizoli@demec.ufmg.br

Abstract. *Thermomagnetic motors are based on the effect of heat on the magnetic properties of magnetic materials. They are interesting if the heat source is a low-grade waste heat, in cogeneration systems, even though they present low Carnot Efficiency when operating in temperature ranges from 25ºC (heat sink) up to 200ºC (heat source). The present work proposes the evaluation and comparison of the Ericsson and Brayton cycles applied to thermomagnetic motors. Gadolinium is considered as the magnetic material and its temperature-entropy diagram, as well magnetization data, were obtained from WDS theory. The analyses are based on the specific work, and the first law and second laws of thermodynamics efficiencies.*

Keywords: *Thermomagnetic motors, magnetic material, thermodynamic cycles, Ericsson Cycle, Brayton Cycle*

1. INTRODUCTION

The global energy demand is currently increasing. According to the World Energy Council (2016), using more efficient energy conversion systems is a way to supply the increasing demand but do not increasing the energy production. One mean to do that, is to recover heat wasted through industrial processes and convert it to a more useful type of energy, such as mechanical or electrical (Forman *et al.*, 2016). The waste of heat can be divided according to its temperature. *High-grade* correspond to temperatures higher than 650ºC; *medium-grade* from 230ºC to 650ºC; and *low-grade* for lower temperatures than 230ºC. However, recovering *low-grade* heat waste is a low efficiency process, and mostly made from solid state thermal energy harvesters (Kishore and Priya, 2020). Among those, thermomagnetic motors and generators can be applied as thermal energy harvesters.

Thermomagnetic motors were initially patented by Nikola Tesla in 1889, but they came back into attention more than a century later, after the discovery of the giant magnetocaloric effect by Pecharsky and Gschneidner (1997). This kind of motors use the effect of heat on the magnetic properties of magnetic materials around their magnetic order transition temperature, or Curie Temperature (T_{curie}) (Kishore and Priya, 2018). Thus, if the material presents Curie Temperature in a range from 20 to 100ºC, it can be applied in a system to recover energy from *low-grade* waste heat (Kishore and Priya, 2017).

There are different motors concepts which converts heat into mechanical energy: with linear or rotary motion; coupled to gravity force, or elastic (spring) force, or magnetic force balance to close the cycle loop (Kitanovski, 2020). Several prototypes according to these concepts have been developed and experimentally tested (Kishore and Priya, 2018). In general, according to the current state-of-the-art, thermomagnetic motors are able to produce high torques, but low powers due to the low operating frequencies. For instance, Takashi *et al.* (2006) built and tested a rotary motor, with three high

field regions, and achieved a maximum power of 3,7 W at a frequency of 0,4 Hz; while Kaneko (2019) built and tested a linear apparatus, and measured of 0,44 W at 0,5 Hz. These motors are among the reported ones with higher powers and frequencies.

Fig. 1 shows schematically the working principle a linear motor coupled to a spring (Kaneko *et al.*, 2019). Initially, Fig. 1(a), the magnetic material (MM) is placed in a low field region (but, higher than 0 T) and it is cooled down by a cold fluid stream from the cold reservoir at T_C. When the MM achieves a temperature lower than T_{curie}, the ferromagnetism is observed and the MM is attracted to the high field region (Fig. 1(b)). The displacement of the MM only happens if the magnetic force gets higher than the spring elastic force. At this position, Fig. 1(c), the MM is heated by a hot fluid stream from a hot reservoir at T_H (which could be supplied from a *low-grade* heat waste). Now, when the MM achieves a temperature higher than T_{curie} (i.e, a non-magnetic phase) and the magnetic force is lower than the spring elastic force, the MM is moved back to the low field region (Fig. 1(d)), restarting the cycle. Thus, it is possible to convert heat into mechanical work.

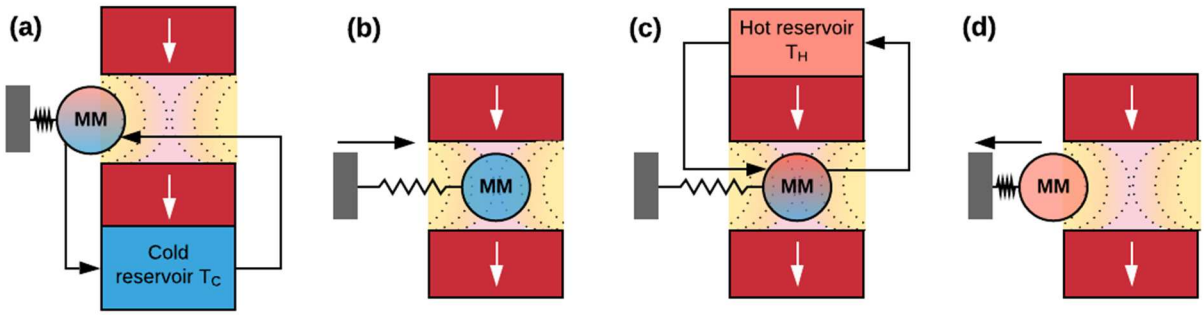

Figure 1. Schematic diagram of the working principle of a linear thermomagnetic motor coupled to a spring system. Adapted from Kaneko et al (2019).

All the concepts of thermomagnetic motors are based on a thermodynamic cycle, mainly Ericsson and Brayton cycles. When compared to the conventional Ericsson and Brayton cycles, thermomagnetic motors replace the gas to a magnetic material (this is why it is called solid state systems), and the isobaric processes to isomagnetic field process. Fig. 2(a) and (b) presents the *T*-*s* diagrams for Ericson and Brayton cycle, respectively.

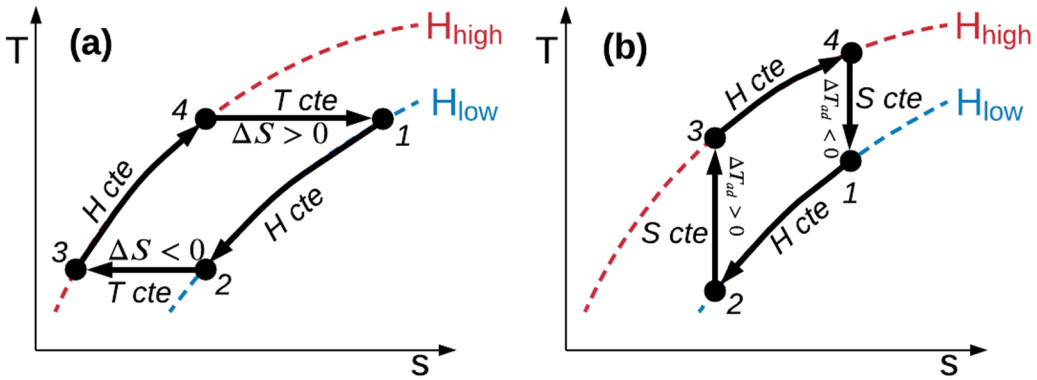

Figure 2. (a) Ericsson Cycle; (b) Brayton Cycle.

The Ericsson cycle is composed by the following steps:

- 1-2: isomagnetic field cooling (corresponds to Fig. 1(a)), the MM is cooled down until $T < T_{curie}$ (heat out);
- 2-3: isothermal magnetization (corresponds to Fig. 1(b)), the MM is moved to the high field region;
- 2-3: isomagnetic field heating (corresponds to Fig. 1(c)), the MM is heated up until $T > T_{curie}$, (heat in);
- 3-4: isothermal demagnetization (corresponds to Fig. 1(d)), the MM is moved back to the low field region;

while the Brayton cycle has the following steps:

- 1-2: isomagnetic field cooling (corresponds to Fig. 1(a)), the MM is cooled down until $T < T_{curie}$ (heat out);
- 2-3: adiabatic magnetization (corresponds to Fig. 1(b)), the MM is moved to the high field region;
- 2-3: isomagnetic field heating (corresponds to Fig. 1(c)), the MM is heated up until $T > T_{curie}$, (heat in);

- 3-4: adiabatic demagnetization (corresponds to Fig. 1(d)), the MM is moved back to the low field region;

Therefore, the differences between the cycles are the processes where the external field is changed: steps 2-3 and 3-4. During these processes the magnetocaloric effect (MCE) is verified (Pecharsku and Gschneidner, 1999; Smith 2013). When the external magnetic field is changed keeping the MM under isothermal conditions, the variation on the magnetic contribution to the total entropy ($\Delta S \equiv \Delta S_M$) represents the MCE; while if the field is changed when the MM is kept under adiabatic conditions, a temperature variation – called adiabatic temperature change (ΔT_{ad}) – represents the MCE.

The main objective of the present work is to evaluate and compare the thermodynamic performance of a thermomagnetic motor operating according to Ericsson and Brayton cycles. The theoretical investigation is developed considering Gadolinium (Gd) as magnetic material. The Curie temperature of Gd is around 20ºC, and it was selected in this study due to the availability of its thermophysical and magnetic properties, read total entropy, magnetization, specific heat and magnetocaloric effect. The Gd properties are evaluated via the Weiss, Debye and Sommerfeld theory. The thermodynamics analyses are based on the specific work, and the first and second laws of thermodynamics efficiencies. Previous works published by Kishore and Priya (2017) and Bessa *et al.* (2018) proposed the thermodynamic evaluation of the Ericsson and Brayton cycles, respectively, but they not performed a comparison between these cycles. Also, Kishore and Priya (2017) evaluated the performance of the motor using different magnetic materials, while Bessa *et al.* (2018) only considered Gd.

2. MODELING

Based on the motor operation and thermodynamics cycles presented in Fig. 1 and 2, the energy interactions along the cycles are: the specific work (w_{liq}), and the specific amount of heat in (q_{in}) and heat out (q_{out}) during the heating and cooling periods. According to the first law of thermodynamics (Moran *et al.*, 2018):

$$w_{liq} = q_{in} - q_{out} \tag{1}$$

In the present theoretical model w_{liq}, q_{in} and q_{out} are evaluated based on the entropy-temperature (*s-T)* diagram of Gd. The total entropy of a magnetic solid can be decomposed into three contributions, the magnetic (s_{mag}), the lattice (s_{lat}) and the electronic (s_{ele}) entropies.

$$s(H,T) = s_{mag}(H,T) + s_{lat}(T) + s_{ele}(T) \tag{2}$$

where s_{mag} is dependent on the temperature (T) and external magnetic field (H), while s_{lat} and s_{ele} are only temperature dependent. Each contribution to the total entropy can be calculated using the Weiss, Debye and Sommerfeld (WDS) Theory (Morrish, 1965; Petersen, 2007).

The Weiss theory, also known as mean field theory, compute the magnetic contribution to the total entropy, given by:

$$s_{mag}(H,T) = \frac{N_A}{M_M} k_B \left[\ln\left(\frac{sinh\left(\frac{2J+1}{2J}\chi\right)}{sinh\left(\frac{1}{2J}\chi\right)} \right) - \chi B_J(\chi) \right] \tag{3}$$

where N_A is the Avogadro number, M_M the Gd molar mass, k_B is the Boltzman constant and J is the total angular momentum. B_J is the Brillouin function, defines as:

$$B_J(\chi) = \frac{2J+1}{2J}\coth\left(\frac{2J+1}{2J}\chi\right) - \frac{1}{2J}\coth\left(\frac{1}{2J}\chi\right) \tag{4}$$

and χ:

$$\chi = \frac{gJ\mu_B\mu_0 H}{k_B T} + \frac{3T_{Curie}J}{T(J+1)} B_J(\chi) \tag{5}$$

therefore, B_J and χ must be solved iteratively, assuming a residual error. Also, g is the Landé factor, μ_B is the Bohr magneton, μ_0 is the vacuum permeability.

Another important magnetic property that is calculated from the mean field theory is the magnetization M:

$$M(H,T) = \rho_s N_s g J \mu_B B_J(\chi) \tag{6}$$

where ρ_s is the density and N_s is the number of magnetic spins per unit of mass.

The Debye theory compute the lattice contribution to the total entropy, given by:

$$s_{lat}(T) = k_B \frac{N_A}{M}\left[-3ln\left(1 - e^{-\frac{\theta_D}{T}}\right) + 12\left(\frac{T}{T_D}\right)^3 \int_0^{\frac{\theta_D}{T}} \frac{x^3}{e^x - 1} dx\right] \tag{7}$$

where θ_D is the Debye temperature.

Finally, the Sommerfeld theory compute the electronic contribution to the total entropy, given by:

$$s_{ele}(T) = \gamma_e T \tag{8}$$

where γ_e is the Sommerfeld constant.

Table 1 shows all the constants and properties respective to gadolinium (Petersen, 2007).

Table 1 – Constant and Gd properties used in the WDS theory.

Property	Value	SI units
T_{Curie}	293	K
M_M	0.157	kg·mol^{-1}
g	2	-
J	3.5	ħ
N_s	3.83·10^{24}	kg^{-1}
θ_D	169	K
γ_e	6.93·10^{-2}	J·kg^{-1}·K^{-2}
k_B	1.38·10^{-23}	J·kg^{-1}
μ_0	4π·10^{-7}	N·A^{-2}
M_B	9.27·10^{-24}	A·m^2
N_A	6.02·10^{23}	mol^{-1}

Fig. 3 presents the *T*-*s* diagram of Gd for different magnetic fields, and Fig. 4 the magnetization as a function of the temperature and the magnetic field. Both results are obtained via the WDS Theory.

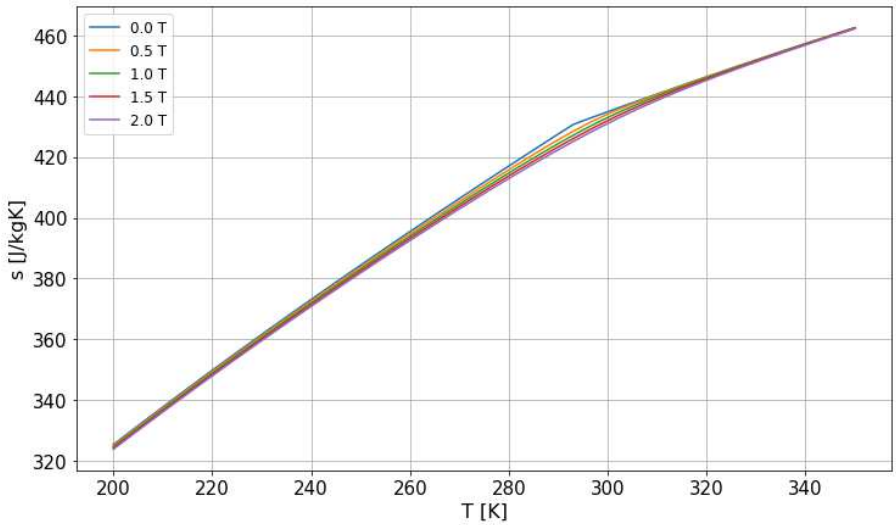

Figure 3. *s*-*T* diagram of Gd for different magnetic fields.

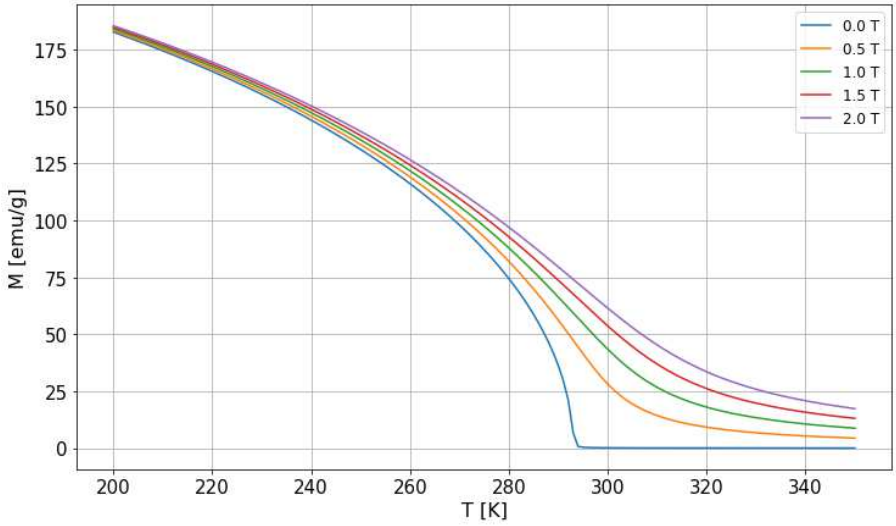

Figure 4. Magnetization of Gd as a function of temperature and magnetic field.

To evaluate q_{in} and q_{out} it was implemented a numerical procedure to calculate the areas stablished under the *s*-*T* diagram as in Fig. 5(a) and (b) for Ericsson and Brayton cycles. Setting the values for the hot and cold reservoirs (T_H and T_C) as well the high and low field intensities (H_{high} and H_{low}), the areas under the *s*-*T* diagram are identified and numerical integrations are performed, as explained next:

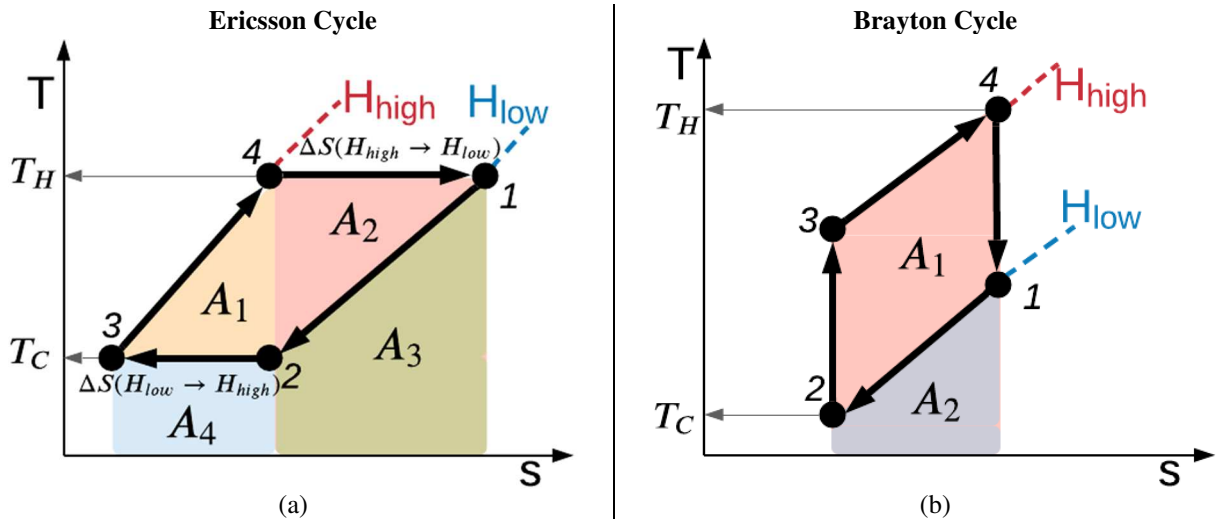

(a) (b)

Figure 5. Schematic diagram presenting the areas stablished under the *s*-*T* diagram: (a) Ericsson cycle; (b) Brayton cycle.

Area 1: $A_1 = \left(\int_{T_C}^{T_H} Tds\right)_{Hhigh}$ (9.1)

Area 2: $A_2 = T_H \Delta s(H_{high} \rightarrow H_{low})$ (9.2)

Area 3: $A_3 = \left(\int_{T_C}^{T_H} Tds\right)_{Hlow}$ (9.3)

Area 4: $A_4 = T_C \Delta s(H_{low} \rightarrow H_{High})$ (9.4)

$q_{in} = A_1 + A_2$ (9.5)

$q_{out} = A_3 + A_4$ (9.6)

Area 1: $A_1 = \left(\int_{T_C}^{T_H} Tds\right)_{Hhigh}$ (10.1)

Area 2: $A_2 = \left(\int_{T_C}^{T_H} Tds\right)_{Hlow}$ (10.2)

$q_{in} = A_1$ (10.3)

$q_{out} = A_2$ (10.4)

Evaluating the Ericsson cycle, ones can see that the heat in (q_{in}) is the sum of the areas A_1 (orange) and A_2 (red), where the area A_1 is respective to the heat absorption from the hot reservoir, while the A_2 is due to the magnetocaloric

effect resultant from the field variation at a fixed temperature T_H ($\Delta s(H_{high} \rightarrow H_{low})$). The heat out ($q_{out}$) is the sum of A_3 (green) and A_4 (blue), where the A_3 is respective to the heat rejection to the cold reservoir, and A_4 is due to the magnetocaloric effect resultant from the field variation at a fixed temperature T_C ($\Delta s(H_{low} \rightarrow H_{high})$). Notice that A_4 overlays A_1, as well A_3 overlays A_2. Another important characteristic is that in a real cycle, respecting the scales and ranges for entropy and temperature, $A_1 \gg A_2$ and $A_3 \gg A_4$.

Next, the Brayton cycle only have two areas, and thus, $q_{in} = A_1$ is the amount of heat absorbed from the hot reservoir, and $q_{out} = A_2$ is the amount of heat rejected to the cold reservoir. Again, A_2 overlays A_1. In Brayton cycle, it is assumed that $T_H = T_4$ and $T_C = T_2$, which means that the MM reaches, ideally, the thermal equilibrium with the thermal reservoirs.

The liquid amount of work produced to both cycles can be further calculated from Eq. (1). Finally, the fist (η_{1st}) and second (η_{2nd}) law efficiencies can be evaluated by (Moran *et al.*, 2018):

$$\eta_{1st} = \frac{w_{liq}}{q_{in}} \tag{11}$$

$$\eta_{2nd} = \frac{\eta_{1st}}{\eta_C} \tag{12}$$

where the Carnot heat engine efficiency is:

$$\eta_C = 1 - \frac{T_C}{T_H} \tag{13}$$

The theoretical evaluation presented in this work assumed fixed values for the applied fields: $H_{low} = 0.5$ T and $H_{high} = 1.5$ T. The reservoirs temperatures, on the other hand, can vary from 230 K to 330 K, but always imposing a minimum temperature difference ($\Delta T = T_H - T_C$) of 1 K up to 100 K. In this analysis, demagnetization losses are disregard.

The mathematical model was implemented in Spyder3 software, utilizing the Python programming language. As explained before, numerical integration methods where used to evaluate the areas. Each numerical integration used 50,000 discrete values of the ordinated pair *s*-*T* to calculate a respective area. An evaluation based on the error's resultant from the numerical integration methods was performed, and the use of 50,000 discrete points guaranteed errors lower than 1% to any simulated condition.

3. RESULTS

Fig. 6 presents the results for Ericsson cycle. The *x*-axis is the hot reservoir temperature, and the *y*-axis is ($\Delta T = T_H - T_C$, where T_H and T_C can vary from 230 to 330 K. Fig. 6(a) shows the results for the heat input; Fig. 6(b) for the specific work produced; Fig. 6(c) for the first law efficiency; and Fig. 6(d) for the second law efficiency. Again, demagnetization losses are not considered in this study. The results here presented for Ericsson cycle are in agreement with Kishore and Priya (2017). Analyzing them, and ones can observe:

- the specific work achieves maximum values from 120 J/kg up to 140 J/kg for $T_H > 300$ K and $\Delta T > 60$ K;
- however, the heat inputs are quite high, achieving values higher than 15000 J/kg for $T_H > 300$ K and $\Delta T > 60$ K;
- as a result, the first law efficiency is small, with maximum values of 0.7%, at $290 < T_H < 320$ K and $10 < \Delta T < 50$ K;
- the second law efficiencies can reach 30% as ΔT decreases.

Fig. 7 presents the results for Brayton cycle. Again, the *x*-axis is the hot reservoir temperature, and the *y*-axis is ($\Delta T = T_H - T_C$, where T_H and T_C can vary from 230 to 330 K, and: (a) shows the results for the heat input; (b) for the specific work produced; (c) for the first law efficiency; and (d) for the second law efficiency. For Brayton cycle, the results are in agreement with Bessa *et al.* (2018), and they show that:

- the specific work achieves maximum values from 120 J/kg up to 140 J/kg for $T_H > 300$ K and $\Delta T > 60$ K;
- again, the heat inputs are quite high;
- as a result, the first law efficiency is small, with maximum values of 0.8%, at $290 < T_H < 320$ K and $\Delta T < 40$ K;
- the second law efficiencies can reach 30% as ΔT decreases.

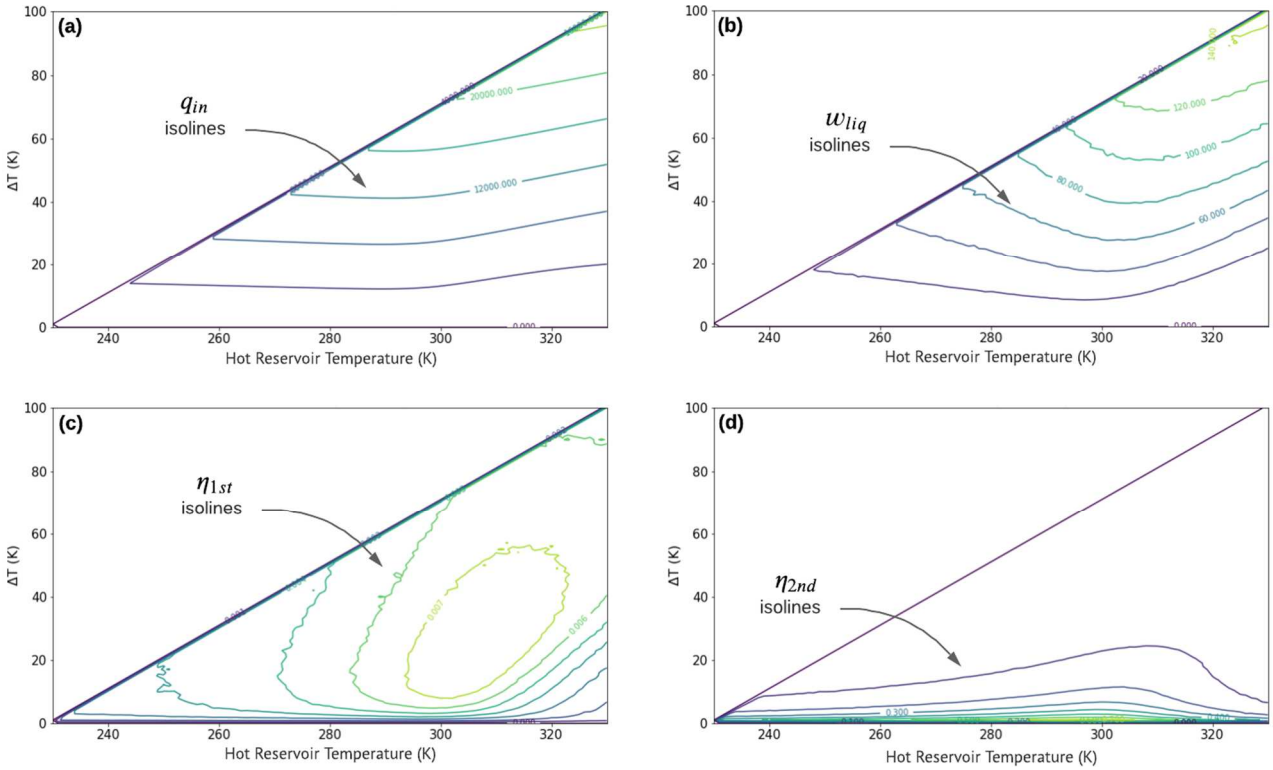

Figure 6: Results for Ericsson cycle as a function of the temperature difference between the thermal reservoirs (ΔT) and hot reservoir temperature: (a) heat input; (b) specific work; (c) first law efficiency; (d) second law efficiency.

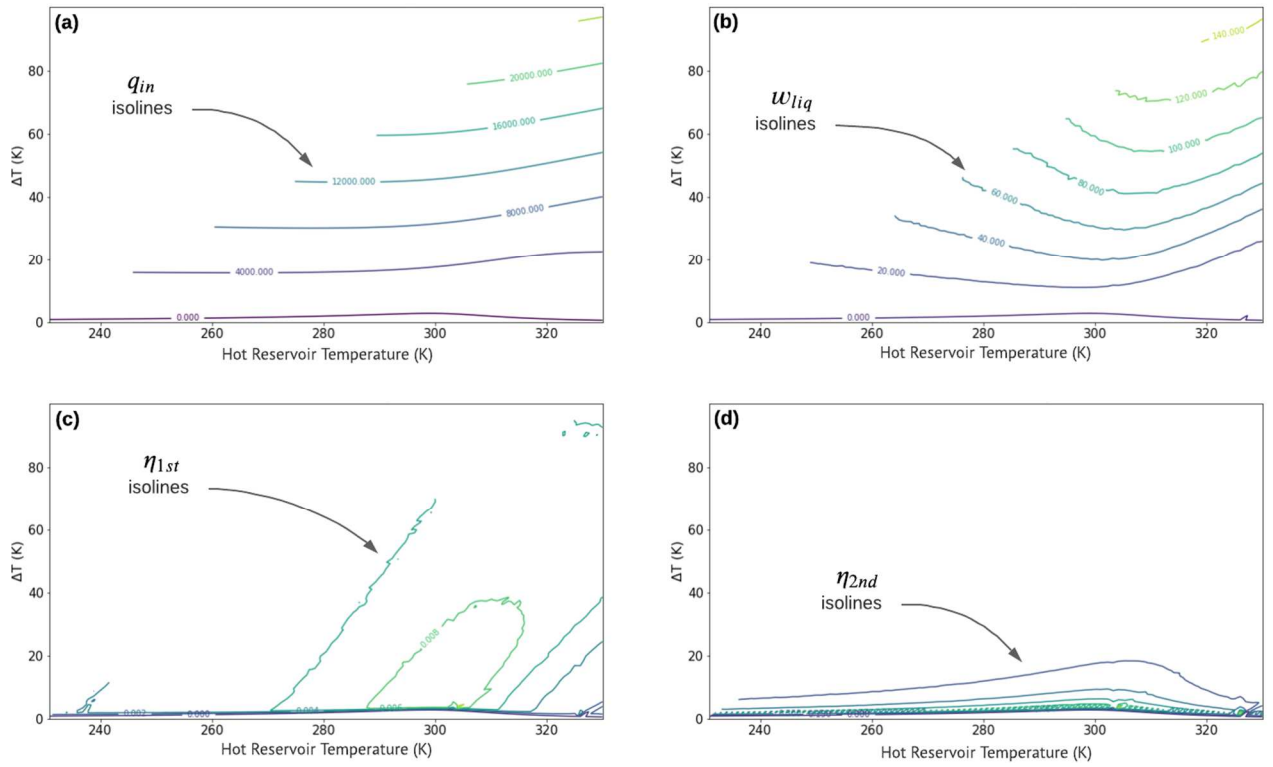

Figure 7: Results for Brayton cycle as a function of the temperature difference between the thermal reservoirs (ΔT) and hot reservoir temperature: (a) heat input; (b) specific work; (c) first law efficiency; (d) second law efficiency.

Comparing the cycles, ones can observe:

- i) the specific work values are similar to both cycles, with maximum values around 140 J/kg;
- ii) the first law efficiency is very low to both cycles, with maximum values around 1%;
- iii) Ericsson cycle presented a more interesting result because, at efficiency values around 1%, the specific work was 50 J/kg, while it was 20 J/kg to Brayton cycle;

4. CONCLUSIONS

This work presented a thermodynamic evaluation of thermomagnetic motors operating according to Ericsson and Brayton cycles. A theoretical model was developed combining the first and second laws of thermodynamics with numerical integration methods applied to *s-T* diagrams of gadolinium to calculate the amount of heat absorbed and rejected along a cycle. The proposed methodology was verified with previously reported results, and a good agreement was found. Thus, further comparisons between the results for Ericsson and Brayton cycles were performed. Ericsson cycle presented a more interesting performance. However both, first and second law efficiencies for the motor using Gd are quite low. Therefore, it is possible to conclude that thermomagnetic motors are interesting when used to recover wasted heat, only if the necessary power input to operate the motor (for instance, pumping power) is much smaller than the power produced by the motor. Future works will include different losses, such as demagnetization losses and non-isothermal or non-adiabatic conditions. Also, different magnetocaloric materials will be studied following the same protocols.

5. ACKNOWLEDGEMENTS

Financial support from CNPq though PIBIC program is duly acknowledged.

6. REFERENCES

Bessa, C. V. X., *et al*., 2018. “On the relevance of temperature, applied magnetic field and demagnetizing factor on the performance of thermomagnetic motors”. *Applied Thermal Engineering*, Vol. 145, pp. 245-250.

Forman, C., *et al.*, 2016. “Estimating Global Waste Heat Potential”. *Renewable and Sustainable Energy Reviews* Vol. 57, pp. 1568-1579.

Kaneko, G. H, 2019. “Projeto e Construção de um Motor Termomagnético do Tipo Tesla”. *Dissertação de mestrado – Programa de pós-graduação em engenharia mecânica*, Universidade Estadual de Maringá.

Kaneko, G. H., *et al*., 2019. “Design and Assembling of a Magnetic Circuit for a Thermomagnetic Motor Apparatus. *Journal of the Brazillian Society of Mechanical Sciences and Engineering*, Vol. 41, pp. 394.

Kishore, R.A. and Priya, S., 2017. “Low-grade waste heat recovery using the reverse magnetocaloric effect”. *Sustainable Energy & Fuels*, Vol. 1(9), pp. 1899-1908.

Kishore, R.A. and Priya, S., 2018. “A review on design and performance of thermomagnetic devices” *Renewable Sustainable Energy Rev*. Vol. 81, pp. 33–44.

Kishore, R.A. and Priya, S., 2020. “Linear thermomagnetic energy harvester for low-grade energy harvesting”. *Journal do Applied Physics*, Vol. 127, pp. 044501.

Kitanovski, A., 2020. “Energy Applications of Magnetocaloric Materials”. *Advanced Energy Materials*, 1903741.

Morrish, A., 1965. *The Physical Principles of Magnetism*. John Wiley & Sons, Inc.

Moran, M.J., *et al.*, 2018. “Fundamentals of engineering thermodynamics”. Wiley.

Pecharsky, V. K., Gschneidner, K. A. Jr., 1999. “Magnetocaloric effect and magnetic refrigeration”. *Journal of Magnetism and Magnetic Materials*, Vol. 200, p. 44–56.

Pecharsky, V.K., Gschneidner Jr., K.A., 1997. “Giant magnetocaloric effect in $Gd_5Ge_2Si_2$”. *Physical Review Letters* Vol. 78, pp. 4494-4497.

Petersen, T. F., 2007. “Numerical modelling and analysis of a room temperature magnetic refrigeration system”. *Dissertação de Mestrado – Fuel Cells and Solid State Chemistry Department*, Technical University of Denmark. Dinamarca.

Smith, A., 2013. “Who discovered the magnetocaloric effect?” *The European Physical Journal H*, Vol. 38(4), pp. 507-517.

Takahashi, Y., Yamamoto, K., Nishikawa, M., 2006. “Fundamental Performance of Triple Magnetic Circuit Type Cylindrical Thermomagnetic Engine”. *Electrical Engineering in Japan*, Vol. 154 (4).

Tesla, N., 1889. US Pat., 396121.

World Energy Council. World Energy Scenarios (2016).

7. RESPONSIBILITY NOTICE

The authors are the only responsible for the printed material included in this paper.